STEM CELLS AND DEVELOPMENT
Volume 23, Number 3, 2014

DOI: 10.1089/scd.2013.0132

Potential of Human Fetal Chorionic Stem Cells for the Treatment of Osteogenesis Imperfecta

Gemma N. Jones,[1,*] Dafni Moschidou,[1,*] Hassan Abdulrazzak,[1] Bhalraj Singh Kalirai,[1] Maximilien Vanleene,[2] Suchaya Osatis,[1] Sandra J. Shefelbine,[2] Nicole J. Horwood,[3] Massimo Marenzana,[2] Paolo De Coppi,[4] J.H. Duncan Bassett,[5] Graham R. Williams,[5] Nicholas M. Fisk,[6] and Pascale V. Guillot[1]

Osteogenesis imperfecta (OI) is a genetic bone pathology with prenatal onset, characterized by brittle bones in response to abnormal collagen composition. There is presently no cure for OI. We previously showed that human first trimester fetal blood mesenchymal stem cells (MSCs) transplanted into a murine OI model (*oim* mice) improved the phenotype. However, the clinical use of fetal MSC is constrained by their limited number and low availability. In contrast, human fetal early chorionic stem cells (e-CSC) can be used without ethical restrictions and isolated in high numbers from the placenta during ongoing pregnancy. Here, we show that intraperitoneal injection of e-CSC in *oim* neonates reduced fractures, increased bone ductility and bone volume (BV), increased the numbers of hypertrophic chondrocytes, and upregulated endogenous genes involved in endochondral and intramembranous ossification. Exogenous cells preferentially homed to long bone epiphyses, expressed osteoblast genes, and produced collagen COL1A2. Together, our data suggest that exogenous cells decrease bone brittleness and BV by directly differentiating to osteoblasts and indirectly stimulating host chondrogenesis and osteogenesis. In conclusion, the placenta is a practical source of stem cells for the treatment of OI.

Introduction

Osteogenesis imperfecta (OI), or brittle bone disease, is a debilitating inherited skeletal dysplasia with prenatal onset that affects 1 in 15,000–20,000 births. OI is characterized by short stature, osteopenia, and multiple fractures. The severity of the disease ranges across the 11 known types depending on the causative mutation in collagen type I or genes involved in its biosynthesis, with type III being the most severe that survive the neonatal period [1–4]. Existing treatments largely provide symptomatic relief, but there is currently no cure. The gold standard bisphosphonates temporarily improve bone strength by inhibiting bone resorption, but they do not improve growth or bone pain beyond a year [5] and do not reduce fracture incidence long term [6].

Cell therapy in OI aims to prevent morbidity and deformity and mortality, by introducing healthy cells, early in development, with the aim that exogenous cells will home to bones and contribute to bone formation to decrease the severity of the disease [7]. Cell therapy for OI holds much promise, with most studies showing beneficial effects. In humans, whole bone marrow and bone marrow mesenchymal stem cells (MSC) have been transplanted in OI children with gains in body length and bone mineralization [8,9], while allogeneic fetal liver-derived stem cells transplanted in utero led to apparent phenotypic improvement in an OI fetus, although confounded by concomitant bisphosphonate use [10]. In rodent OI models, transplantation of whole bone marrow/bone marrow MSC led to increased collagen content [11], improved bone strength, reduced perinatal lethality [12], and increased osteoblast differentiation [13,14]. Marked therapeutic benefits were shown following transplantation of fetal MSC from human first trimester blood in a mouse model of human type III OI (*oim*) including improved bone plasticity and a two-third reduction in long bone fractures [15,16].

However, there are a number of hurdles to overcome before fetal stem cell therapy can be translated to the clinic. For example, it is essential to have a source of stem cells that have high therapeutic potential and are easily accessible for clinical use. Extra-embryonic fetal tissues, such as the placenta, are readily available either from termination of

[1]Institute of Reproductive and Developmental Biology, Imperial College London, London, United Kingdom.
[2]Department of Bioengineering, Imperial College London, London, United Kingdom.
[3]Kennedy Institute of Rheumatology, Imperial College London, London, United Kingdom.
[4]Surgery Unit, UCL Institute of Child Health, London, United Kingdom.
[5]Molecular Endocrinology Group, Department of Medicine, Imperial College London, London, United Kingdom.
[6]UQ Centre for Clinical Research, University of Queensland, Brisbane, Australia.
*These authors equally contributed to this study.

pregnancy or surplus tissue at routine prenatal diagnostic procedures [17,18], or at term delivery [19,20–22]. Recently, we have shown human fetal early chorionic stem cells (e-CSC) isolated from human placental tissue accelerated tissue repair in dermal excision skin wounds and improved bone quality and plasticity in *oim* mice. This tissue repair capacity of e-CSC was greater than its late gestation counterparts in vivo, as was the osteogenic differentiation and cell expansion potential in vitro [23]. This may be due to the more primitive characteristics of e-CSC compared to term isolated CSC, which showed an intermediate phenotype between human embryonic stem cells (hESCs) and MSC [23].

We hypothesized that transplantation of stem cells derived from first trimester placenta would have therapeutic benefits in a mouse model of OI. Here, we show that exogenous e-CSC engrafted at sites of bone growth and repair in the *oim* model, differentiated to osteoblasts that produced COL1A2 and mediated changes in endogenous ossification genes, which resulted in reduced fractures and increased bone flexibility.

Materials and Methods

Cells

Collection of human fetal early chorionic stem cells (e-CSC) was as previously described [23] from first trimester chorionic villous tissue sampled during pregnancy termination (9–10 weeks gestation age) as approved by the Research Ethics Committee of Hammersmith and Queen Charlotte's Hospital. Isolated cells were plastic adherent and cultured in Dulbecco's modified Eagle's medium high glucose (DMEM-HG) (Sigma) supplemented with 10% fetal bovine serum (BioSera), 2 mM L-glutamine, 50 IU/mL penicillin, and 50 mg/mL streptomycin (Gibco-BRL) (D10 medium). Cells were expanded at 70%–80% confluence on plastic dishes and used at passage 6–8.

The chondrogenic ATDC5 cells (generous gift from J.H. Duncan Bassett and Graham R. Williams) were expanded in D10 medium. Differentiation was chemically induced by culturing the cells with 10 ng/mL TGF-β3, 1×ITS (insulin, transferrin, selenium), 10 nM dexamethasone, and 100 μM ascorbate-2-phosphate for 7 days.

Fluorescence immunostaining and confocal microscopy

Human e-CSC were fixed in 4% then 8% PFA in 125 mM HEPES (pH7.6), then permeabilized in 0.5% Triton X-100 (Sigma), incubated with 20 μM glycine (Sigma), and blocked in phosphate-buffered saline (PBS) supplemented with 1% bovine serum albumin (BSA), 0.2% gelatin, and 0.1% casein (pH7.6). Cells were stained with primary antibodies (listed in Supplementary Table S1; Supplementary Data are available online at www.liebertpub.com/scd) then secondary antibody; donkey anti-mouse or anti-rabbit IgG (Jackson ImmunoResearch Laboratories), before being mounted in VectaShield labeled with DAPI (Vector Labs) [24]. Fluorescence confocal laser scanning microscopy images were collected on a Leica TCS SP5 (X1000 PL APO oil objective). Positive controls were hESC and negative controls differentiated cells.

Flow cytometry

Cells were detached, blocked with PBS supplemented with 1% BSA (Sigma), and either fixed in 0.01% PFA and permeabilized with 0.5% Triton X-100 for intracellular staining, or immediately stained with primary antibodies for cell surface staining (Supplementary Table S1). For unconjugated antibodies, cells were subsequently washed with 1% BSA and incubated with secondary goat anti-murine IgM PE (Santa Cruz) [23]. Otherwise cells were analyzed by FACS calibur flow cytometry (Becton Dickinson) using hESC as positive and antibody-specific isotypes as negative controls.

Cell differentiation

Cells were differentiated along the osteoblast lineage for 2 weeks in DMEM-LG supplemented with 10 mM β-glycerophosphate, 0.2 mM ascorbic acid, and 10^{-8} M dexamethasone, then fixed in 10% formalin and stained with von Kossa (2% silver nitrate) or 2% alizarin red. Cells were differentiated along the adipocyte lineage over 2 weeks in DMEM supplemented with 0.5 mM hydrocortisone, 0.5 mM isobutyl methylxanthine, and 60 mM indomethacin, then fixed and stained with oil red O [23]. Cells were differentiated along the chondrocyte lineage over 2 weeks in DMEM-LG supplemented with 0.01 μg/mL TGF-β3, 0.1 μM dexamethasone, 0.17 mM ascorbic acid, 1 mM sodium pyruvate, 0.35 mM L-proline, 1% ITSS, and 50 μg/mL linoleic acid (reagents from Sigma), then cells were fixed in and stained with alcian blue (2%).

Animals

All experimental protocols complied with Home Office guidelines (PPL 70/6857). Heterozygous male and female (B6C3Fe a/a-Col1a2^{oim}/Col1a2^{oim}) mice (Jackson Laboratory) were housed in individual ventilated cages in 12:12-h light–dark cycle (21°C) with water and chow. Offspring were genotyped by sequencing the *oim* fragment then homozygous and wild-type colonies were established. Progeny were weaned at 30±1 day and culled at 8 weeks of age. Human e-CSC (10^6 cells resuspended in 20 μL of cold PBS) were injected intraperitoneally (i.p.) into 3–4-day-old *oim* neonates ($n=11$ males and $n=11$ females) and mice were culled for analysis when they were 8-week-old. We noted no variability between different isolated placenta specimens in terms of e-CSC phenotype (data not shown) and donor cells injected in *oim* mice were from a single donor. Controls comprised age-matched nontransplanted *oim* and wild-type mice.

Immunohistochemistry

Dissected tibias were decalcified in 10% EDTA pH7.4 and subsequently embedded in paraffin. Four micron sections were cut, deparaffinized in xylene, and rehydrated. Heat-induced epitope retrieval was performed in a steamer (Dako), followed by incubation with peroxidize block (Dako). The presence of donor cells in transplanted 8-week-old *oim* mice was determined in three different regions of the nonfractured tibia (epiphysis, diaphysis, and bone marrow) and in fracture callus. Donor cells were visualized using human-specific mouse monoclonal vimentin (Dako) primary antibody (Supplementary Table S1) and

incubated with HRP-labeled anti-mouse polymer followed by DAB+substrate-chromogen staining. Positive cells were counted in bone marrow ($n=4$ samples and $n=4$ sections for each). Staining specificity was verified using nontransplanted negative controls.

Detection of Collagen type X and Osteopontin (Supplementary Table S1) was performed on 4 μm sagittal sections of tibia from 8-week-old mice, using HRP-labeled polymer followed by DAB+ substrate-chromogen staining.

Engraftment measured by quantitative real-time PCR

Femurs of the same mice were dissected and separated into callus if present ($n=8$), epiphysis ($n=6$), and diaphysis ($n=6$). Liver ($n=6$) was also used. RNA was then extracted using TRIzol (Invitrogen) followed by cDNA synthesis with M-MLV reverse transcriptase (Promega). To calculate donor cell engraftment quantitative real-time PCR (qPCR) was performed using SYBR green dye (Applied Biosystem) and the ABI Prism 7700 Sequence Detection System with human-specific and human-mouse nonspecific *β-actin* primers (Supplementary Table S2). Human:mouse chimerism was estimated as the ratio of human *β-actin* to total human and mouse *β-actin* in the total cDNA sample to give the $2^{-\Delta Ct}$ value. Samples were considered positive with a human-specific *β-actin* Ct above 36 at a threshold of 0.13ΔRn. Negative controls were nontransplanted *oim* [15].

Quantitative real-time RT-PCR

Osteoblast gene expression was performed by quantitative real-time RT-PCR (qRT-PCR) using SYBR green dye (Qiagen) and the MJ-Opticon with human-specific *Osteopontin* and *Osteocalcin* primers (Supplementary Table S2). Results with a Ct below 36 were normalized to human *β-actin* to give the $2^{-\Delta Ct}$ value. Expression in transplanted *oim* femurs ($n=6$) was compared to e-CSC ($n=3$) undifferentiated and grown in osteogenic permissive media for 2 weeks. Negative controls were nontransplanted *oim* [15]. *Sox9* expression in ATDC5 cells was measured by qRT-PCR using the $2^{-\Delta Ct}$ method. Manufactured mouse-specific primers were from SABiosciences (Qiagen).

Western blot

Collagen was extracted from ground bone over 72 h at 4°C in a lysis buffer of 6 M guanidine HCl and 100 mM Tris pH7.4 containing protease inhibitor cocktail. Proteins were precipitated with 10% TCA, resuspended in RIPAE buffer (1×TBS, 1% Nonidet P-40, 0.5% sodium deoxycholate, 0.1% sodium dodecyl sulfate (SDS), and 0.004% sodium azide; Sigma) containing PMSF (Sigma) and protease inhibitor cocktail, run on an 8% SDS-PAGE, transferred to nitrocellulose, blocked with milk, and stained with a COL1A2 (129 kDa) primary antibody (Abcam), then with an HRP-linked anti-rabbit IgG secondary antibody (GE Healthcare), followed by enhanced chemiluminescence detection (Thermo Scientific). The loading control used was β-ACTIN (43 kDa) (Santa Cruz) [23]. Detection of COL1A2 in transplanted *oim* bones was confirmed using wild-type positive controls and specificity confirmed using nontransplanted *oim* negative controls ($n=4$ per group).

Mechanical testing

Three-point bending tests were performed as described [23] using a materials testing machine (5866 Instron) on 8-week-old unfractured frozen and thawed femurs ($n=22$ transplanted *oim*, $n=34$ *oim* controls, and $n=14$ wild-type). Bones were bent mid-diaphysis to fracture on two supports 9 mm apart at a loading rate of 50 μm/s. Force deflection curves were analyzed (Matlab; MathWorks) to measure bending stiffness (slope of the linear elastic deformation; N/mm), load to fracture (maximum force sustained prior to fracture; N), and maximum deflection (deflection at fracture in mm).

X-ray microradiography

Tibias from 8-week-old mice ($n=19$ transplanted, $n=20$ *oim*, and $n=11$ wild-type) were fixed in formalin for 24 h and stored in 70% ethanol prior to removal of soft tissues. Digital X-ray images were obtained at a 10-μm pixel resolution using a Faxitron MX20 variable kV point projection X-ray source and digital image system (Qados, Cross Technologies plc). An X-ray image of a digital micrometer was used to calibrate ImageJ 1.41 software (http://rsb.info.nih.gov/ij/) prior to determination of cortical bone thickness and diameter at five locations along the mid shaft, and bone length. Relative bone mineral content (BMC) was determined by comparison with 1 mm diameter steel, aluminium, and polyester standards included in each frame. Sixteen bit DICOM images were converted to 8-bit Tiff images using ImageJ and the image histogram stretched between the polyester (gray level 0) to steel (gray level 255) standards. Bone mineralization densities were represented by a pseudocolor scheme representing 16 equal intervals [25].

Counting of fractures

Fractures in both femurs, tibias, and humeri were assessed at 8 weeks of age by determination of callus formation ($n=120$ transplanted and $n=78$ *oim* control). The number of mice with at least one long bone fracture and the fracture incidence (number of fractured bones/total bones assessed) were calculated by two independent observers blinded to transplantation status. Deformities and callus formation in the caudal vertebrae ($n=16$ transplanted and $n=10$ *oim* control) were counted on digital X-ray images and the fracture rate was calculated as above. The presence of vertebral deformity and callus formation detected by X-ray microradiography was verified by micro computerized tomography (μCT40; Scanco Medical) at 10 μm voxel resolution (45 kV, 177 μA, 200 ms integration time). Unfractured *oim* vertebrae did not differ in shape from wild-type vertebrae (Supplementary Fig. S1A) and had normal morphology (Supplementary Fig. S1B), while deformed vertebra had evidence of callus formation (Supplementary Fig. S1C, D) [16].

Dynamic histomorphometry

Animals ($n=7$ transplanted, $n=6$ wild-type, and s$n=5$ *oim*) were injected 10 and 3 days before sacrifice with 20 mg/kg of calcein (Sigma). Tibias were then fixed in formalin for 24 h and transferred to 70% ethanol, before being dehydrated in acetone for 48 h, infiltrated over 6–9 days at −20°C, and

embedded in methylmethacrylate (MMA) [26]. Embedded samples were imaged on a Leica TCS SP5 confocal laser scanning microscope and analyzed using ImageJ. Fluorescent images of calcein labels were taken 500 and 1,000 μm below the proximal growth plate of the trabecular and endocortical regions respectively The amount of mineralizing surface per total bone surface (MS/BS; %), the daily mineral apposition rate (MAR; μm/day), and the bone formation rate (BFR; $\mu m^3/\mu m^2$/day) were calculated.

Static histomorphometry

MMA embedded samples were cut into 8 μm sections and stained using the Leucognost AP kit (Merck), according to the manufacturer's instructions ($n=6$ transplanted, $n=6$ *oim*, and $n=5$ wild-type). Sections were analyzed on a light microscope using the Osteomeasure system (OsteoMetrics, Inc.). Histomorphometric measurements of the secondary spongiosa were performed on stained sections 500 μm from the end of the hypertrophic zone of the growth plate; % trabecular bone volume per total tissue volume (BV/TV) was quantified. For growth plate analysis dissected tibia were decalcified; paraffin embedded; 5 μm sections were cut and stained with alcian blue 8GX (2%), Weigert's hematoxylin, and van Gieson; and mounted and growth plate morphology analyzed using ImageJ ($n=14$ transplanted *oim*, $n=5$ *oim*, and $n=5$ wild-type).

Osteogenesis PCR array

Total RNA was extracted from femoral epiphysis of 8-week-old mice using TRIzol (Invitrogen), followed by RNA clean up (RNeasy Qiagen) and cDNA synthesis using an RT^2 First Strand Kit (Qiagen). Gene expression was investigated using an RT^2 Profiler mouse osteogenesis PCR array (Qiagen) and analyzed according to the manufacturer's instructions ($n=3$ mice per group). To verify results, quantitative real-time PCR was performed using RT^2 qPCR Master Mix and primers (Supplementary Table S2) and analyzed with MJ-opticon (Biorad). Data were normalized to two housekeeping genes (*β-Actin* and *Hsp90ab1*) and the $2^{-\Delta Ct}$ of each sample calculated ($n=8$ transplanted *oim* and $n=5$ *oim* controls).

Protein measurement

Cells were cultured either in D10 medium (nonprimed) or in co-culture without cell contact with ATDC5 cells (primed with ATDC5) or in the presence of blood serum from *oim* or wild-type mice (primed with *oim* or WT serum) for 7 days. The mouse cell line ATCD5 is chondrogenic and goes through a sequential process analogy to chondrocyte differentiation, constituting an excellent in vitro model cell line for analyzing skeletal development and studying the factors involved in chondrogenesis [27]. The presence of protein was measured in the medium using Mini ELISA development kits (Peprotech) for the detection of human-specific basic fibroblast growth factor (bFGF), platelet-derived growth factor-BB (PDGF-BB), and connective tissue growth factor (CTGF), following the manufacturer's protocol. Briefly, ELISA microplates (Corning) were incubated overnight with capture antibody, washed with 0.05% Tween-20 in PBS (Sigma), incubated with standards or samples for 2 h, washed and incubated with detection antibody for 2 h, followed by washing and incubation with Avidin-HRP conjugate for 30 min. Finally, substrate was added to the wells and color development was monitored at 405 nm with wavelength correction set at 650 nm. For the detection of human factor IX in blood serum of transplanted *oim* mice, a kit containing microplates precoated with antibody was used (Abcam), using the protocol recommended by the manufacturer. Detection was carried out at 450 nm.

Statistical analysis

Data were expressed as mean ± SEM (standard error). Normally distributed data were analyzed by unpaired two-tailed Student's *t*-test or one-way ANOVA followed by a Tukey's multiple comparison post hoc test. $P<0.05$ was considered significant. Two-tailed 2×2 Fisher exact was used for categorical comparisons. Cumulative frequency distributions of bone mineral densities were compared using the Kolomogorov–Smirnov test. Chi-squared with Yates correction and to one degree of freedom was used to compare fracture incidence.

Results

Characterization of e-CSC

The e-CSC transplanted in neonatal *oim* have a pre-pluripotent phenotype as previously described [23], showing some characteristics of both MSC [28] and hESCs [29,30]. MSC traits were demonstrated by positive expression of adhesion molecules CD29 and CD44, and the MSC-associated markers CD73, CD90, and CD105, and absent expression of the endothelial or hematopoietic markers CD14, CD34, and CD45, while presenting low levels of intracellular HLA I and no expression of HLA II, similar to fetal liver MSC [31] (Fig. 1A). A sub fraction of cells expressed key hESC markers required for the maintenance of pluripotency; OCT4A, SOX2, TRA-1-60, and SSEA4 (Fig. 1B, C) As expected, e-CSC showed tri-lineage differentiation capability; osteogenic differentiation by alizarin red staining of calcium deposits and von kossa staining of mineralization, chondrogenic differentiation by Safranin O staining of cartilage matrix, and adipogenic differentiation by oil red O staining of lipid droplets (Fig. 1D).

Bones of transplanted mice are less liable to fracture

Eight weeks after e-CSC were transplanted, 11/20 *oim* mice (55%) had no long bone (femur, tibia, and humerus) fractures, whereas all nontransplanted *oim* controls (100%; $n=13$) had at least one or more long bone fracture (Fig. 2A). The fracture incidence in long bones, calculated as the number of fractured tibia, femur, and humeri over the total number of these bones, was reduced from 29.5% (23/78 total bones) in nontransplanted *oim* to 10.0% (12/120 total bones) in e-CSC transplanted *oim*. This corresponds to a 66% decrease in fracture rate ($X^2=21$, $P<0.001$) (Fig. 2B).

We next counted the number of caudal vertebra fractures on digital X-ray, with a fracture classified as any vertebra having a callus or evidence of bone remodeling (see Supplementary Fig. S1 and Materials and Methods section for

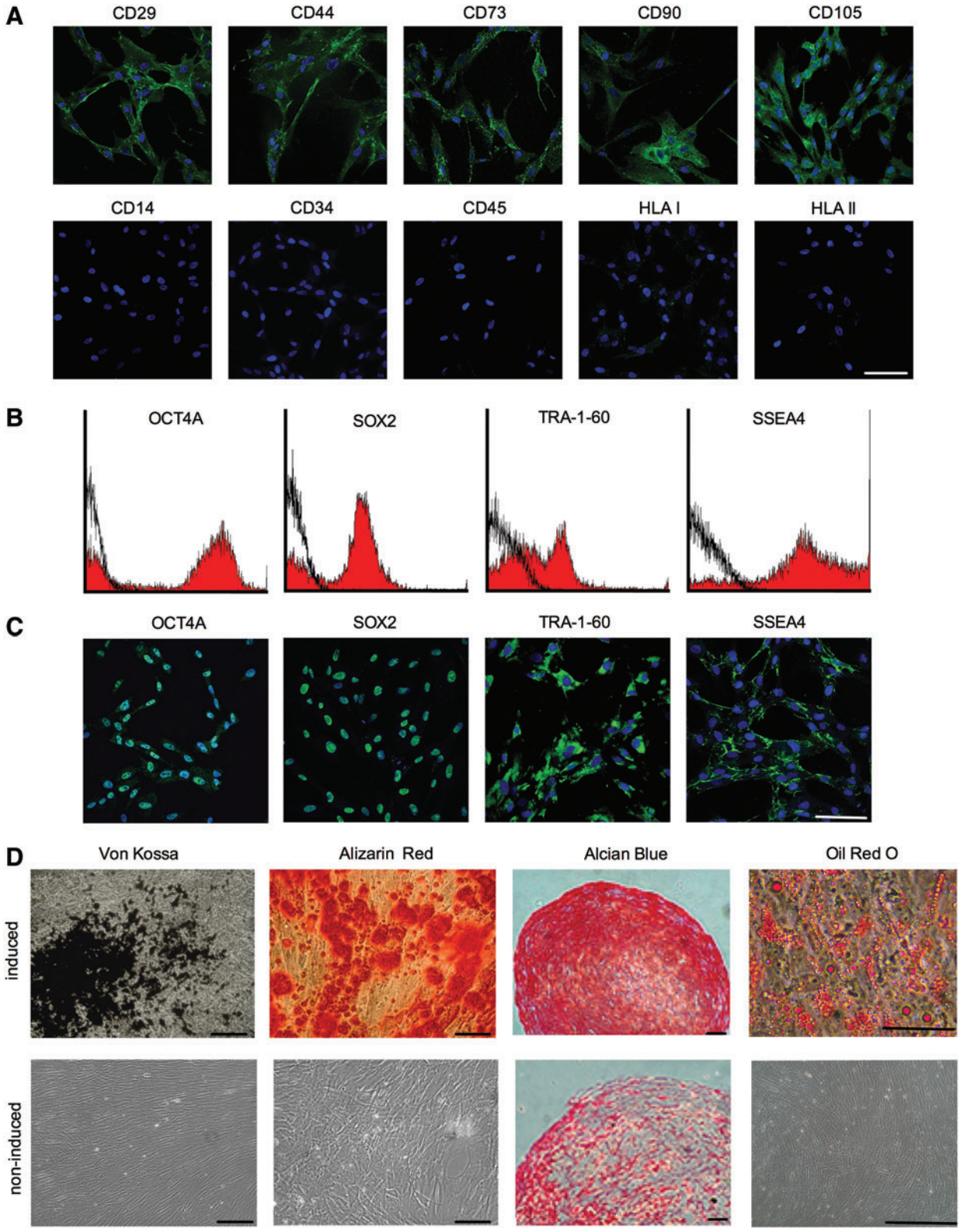

FIG. 1. Early fetal chorionic stem cells (e-CSC) express mesenchymal stem cell (MSC) and human embryonic stem cell (hESC) markers and differentiate down mesenchymal lineages **(A)** Representative confocal immunofluorescence images for expression (*green*) of adhesion molecules (CD29 and CD44), MSC-associated markers (CD73, CD90, and CD105), endothelial marker (CD14), hematopoietic markers (CD34 and CD45), and MHC antigens (HLA I and II). Nuclei stained with DAPI (*blue*). **(B)** Flow cytometry for percent of e-CSC population positive for OCT4A, SOX2, TRA-1-60, and SSEA4 (isotype control in *black*). **(C)** Confocal images for expression of OCT4A, SOX2, TRA-1-60, and SSEA4 in the e-CSC whole population. **(D)** von Kossa staining of calcium mineralization and alizarin red staining of mineralizing nodules following osteogenic differentiation of e-CSC. Safranin O staining of cartilage matrix following chondrogenic differentiation. Oil red O staining of lipid droplets following adipogenic differentiation. Samples were either cultured in the presence of differentiation medium (induced) or in growth medium (un-induced, negative controls). All scale bars 100 μm. Color images available online at www.liebertpub.com/scd

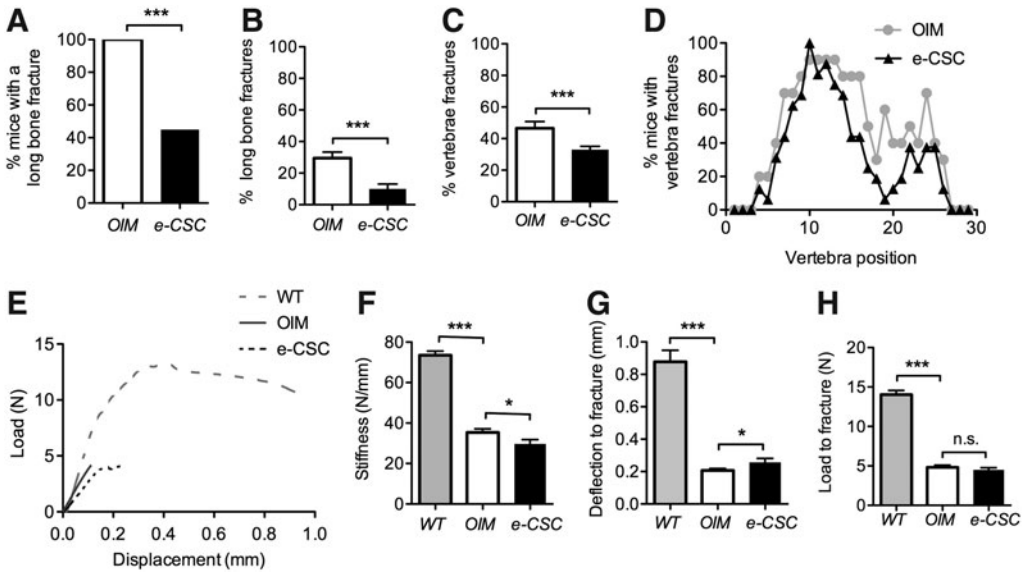

FIG. 2. Transplanted *oim* show improvement in disease pathology. **(A)** Percentage of mice with any long bone fracture. **(B)** Fracture rate; total proportion of fractured femurs, tibias, and humeri over total number of these bones per mouse. **(C)** Percentage caudal vertebral fractures calculated over total number of vertebrae per mouse. **(D)** Percentage of mice with vertebral fractures shown per caudal vertebra from the base of the tail (vertebra number 1) to the tip of the tail (vertebra number 30). **(E)** Three-point bending load (N) displacement (mm) curves shown up to the critical fracture point. **(F)** Bending stiffness of femurs (slope of the linear elastic deformation; N/mm). **(G)** Maximum deflection at fracture (displacement extension to the point of fracture; mm). **(H)** Load to fracture (maximum force sustained by femur prior to fracture; N). All mice were 8 weeks old and wild-type (WT; *gray*), nontransplanted *oim* (OIM; *white*), or e-CSC transplanted *oim* (e-CSC; *black*). ns, not significant; $*P<0.05$, $***P<0.001$; Student's *t*-test or Fisher exact test. Error bars ± SEM.

classification of normal and fractured vertebra by μCT). Compared with nontransplanted *oim* ($n=10$), which showed an average 46.6% ± 4.2% incidence of fractured vertebra per mouse, transplanted mice ($n=16$) had 29.2% fewer vertebral fractures at an average incidence of 33.0% ± 2.2% per mouse ($X^2=33.8$, $P<0.001$) (Fig. 2C). The reduction of vertebral fractures from the nontransplanted control group was widespread, with overall numbers of vertebrae with callus reduced across the majority of vertebral positions (Fig. 2D). Most fractures were found in proximal caudal vertebrae, where force is exerted when rearing up to feed.

Transplanted mice have bones with reduced stiffness and increased ductility

We previously reported three-point bending data from femurs of *oim* mice transplanted with either (e-CSC) or late (l-CSC) gestation CSC [23]. Mice transplanted with e-CSC had greater plasticity and overall bone quality than l-CSC transplanted or control *oim* due to an increased post-yield strain. Here, we further analyzed the three-point bending load–displacement curves to show that e-CSC transplanted *oim* were also more ductile due to a reduction in stiffness in the pre-yield region and an increase in maximum deflection before fracture (Fig. 2E). Bone stiffness of e-CSC transplanted *oim* was reduced by an average of 16% compared with nontransplanted *oim* femurs (29.7 ± 2.1 N/mm SEM vs. 35.3 ± 1.7 N/mm SEM respectively, $P<0.05$) (Fig. 2F), while the maximum deflection was increased in transplanted compared with control *oim* by an average of 24% (0.26 ± 0.02 mm SEM vs. 0.21 ± 0.01 mm SEM, $P<0.05$ respectively) (Fig. 2G). However, the maximal load sustained by transplanted and nontransplanted *oim* femurs prior to fracture was similar (4.5 ± 0.3 N vs. 4.8 ± 0.3 N) (Fig. 2H). In contrast, wild-type compared to *oim* bones were stiffer (73.6 ± 2.0 N/mm, $P<0.001$) (Fig. 2F), with greater maximum deflection (0.88 ± 0.07 mm, $P<0.001$) (Fig. 2G) and sustained higher loads before fracture (14.0 ± 0.5 N, $P<0.001$) (Fig. 2H). Thus, the material properties of bones from transplanted *oim* were not intermediate between the properties of wild-type and *oim* bone. Instead, bones from transplanted *oim* were of strength similar to nontransplanted *oim*, but they displayed greater plasticity and ductility, which may explain their reduced fracture susceptibility.

Transplanted e-CSC preferentially home to oim *epiphysis*

We first performed an ELISA for human factor IX in blood serum of transplanted mice. Results showed absence of mouse anti-human antibodies, indicating an absence of immune reaction of the neonatal murine immune system (data not shown).

Donor cells were visualized by immunohistochemistry in 8-week-old e-CSC transplanted *oim* using a rabbit monoclonal to human vimentin. Staining was localized at the epiphysis, diaphysis, and sites of fracture callus, with some cells present in the primary spongiosa below the growth plate (Fig. 3A). Quantitative real-time PCR (qRT-PCR) showed that donor cell engraftment in transplanted *oim* was highest in the epiphysis, the site of active bone formation. This was 7.1-fold ($P<0.001$) higher than in the nonfractured diaphysis where bone formation is less active, and 11.7-fold ($P<0.01$) higher than engraftment in the liver (Fig. 3B).

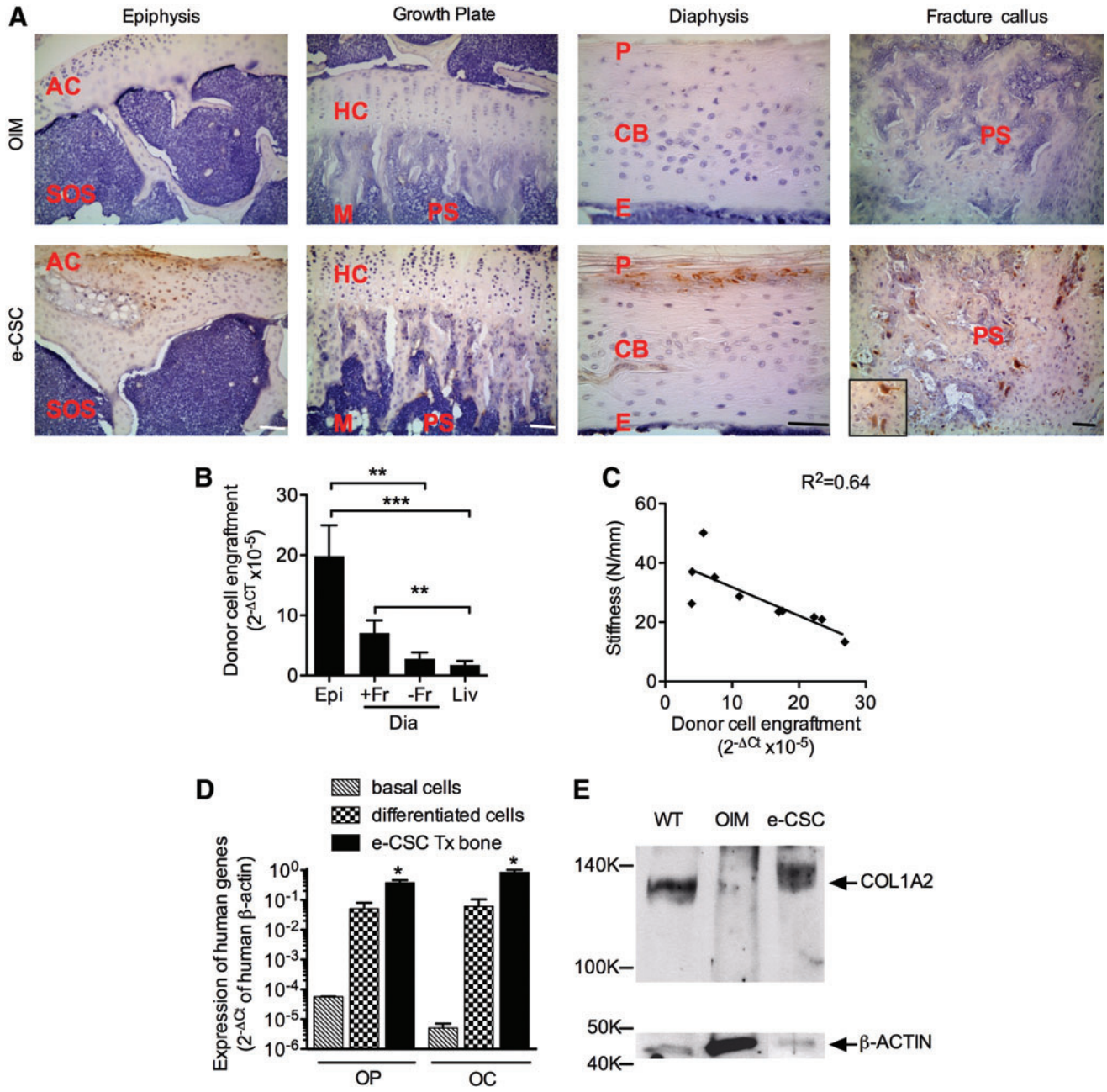

FIG. 3. Transplanted e-CSC engraft and differentiate to osteoblasts in *oim* bone. **(A)** Visualization of human donor cells with DAB staining (*brown*) of human-specific vimentin in the tibial epiphysis, growth plate, diaphysis, and fracture callus of *oim* neonatally transplanted with e-CSC, compared to age-matched nontransplanted *oim* controls. Zoomed in human MSC in the fracture callus shown. Nuclei counter stained with hematoxylin (*blue*). AC, articular cartilage; SOS, secondary ossification site; HC, hyaline cartilage; M, metaphysic; PS, primary spongosia; P, periosteum; CB, cortical bone; E, endosteum. Scale bars all 100 μm. **(B)** Quantitative real-time PCR of donor cell engraftment calculated as the $2^{-\Delta Ct}$ of human-specific *β-actin* normalized to human-mouse nonspecific *β-Actin* in the femoral epiphysis (Epi) and diaphysis (Dia); with (+Fr) and without fracture callus (−Fr), and in the liver (Liv). $^{*}P<0.05$, $^{**}P<0.01$, $^{***}P<0.001$; one-way ANOVA followed by Tukey's post hoc test. Error bars are SEM. **(C)** Linear correlation and regression equation for donor cell engraftment ($2^{-\Delta Ct}$) in the femoral epiphysis per mouse against femur stiffness (N/mm) calculated from the three-point bending test. Linear line of best fit given. **(D)** Quantitative real-time PCR of expression of human-specific *Osteopontin* (OP) and *Osteocalcin* (OC) normalized to human-specific *β-Actin* ($2^{-\Delta Ct}$) in the femurs of e-CSC transplanted oim (e-CSC Tx bone; *black*) and compared to the basal expression level of e-CSC (basal cells; *stripes*) and expression level of cells grown in osteogenic permissive media for 2 weeks (differentiated cells; *checks*). $^{*}P<0.05$; one-way ANOVA followed by Tukey's post hoc test. Error bars are SEM. **(E)** Western blot of expression of COL1A2 protein in the femurs of e-CSC transplanted *oim* (e-CSC) compared to age-matched wild-type (WT) control and nontransplanted *oim* (OIM). Loading control is GAPDH. Color images available online at www.liebertpub.com/scd

Donor cells also preferentially homed to sites of bone repair, where engraftment was fourfold ($P<0.01$) higher than engraftment in the liver. Engraftment in fractured and nonfractured diaphysis were not significantly different, but interestingly more mice were positive for human cDNA in the diaphysis if a fracture callus was present; 90% compared to 60%. Engraftment within the femoral epiphysis was inversely correlated ($R^2=0.64$, $y=-0.96\times+41.43$, $P<0.01$ deviation from zero) with bone stiffness, indicating that bone flexibility increases with increasing numbers of donor cells (Fig. 3C).

Exogenous cells undergo osteogenic differentiation in vivo

To determine whether transplanted cells underwent osteogenic differentiation in vivo expression using qRT-PCR was determined for human-specific *Osteopontin* (*OP*); a major interfacial noncollagenous extracellular matrix proteins found in bone and secreted by osteoblasts [32] and also for *Osteocalcin* (*OC*); an osteoblast-specific gene [33] with an important role in osteoblast differentiation [34]. Results showed expression of human *OP* and *OC* in the transplanted mouse bones ($0.38\pm0.08\cdot2^{-\Delta Ct}$ SEM and $0.85\pm0.18\cdot2^{-\Delta Ct}$ SEM, respectively), which was greater than expression in e-CSC after growth in osteogenic permissive media for 2 weeks ($0.05\pm0.03\cdot2^{-\Delta Ct}$, $P<0.05$ and $0.06\pm0.04\cdot2^{-\Delta Ct}$, $P<0.05$, respectively) and greater than the low/null basal expression level of the undifferentiated cells (Fig. 3D). Western blot analysis showed the COL1A2 protein, missing in nontransplanted *oim* [35], was present in the femoral bones of *oim* transplanted with e-CSC (Fig. 3E), which demonstrates osteogenic differentiation of donor cells to functional osteoblasts.

Transplantation of e-CSC did not affect bone length or cortical bone formation

Tibial length was unaffected by transplantation being similar in transplanted *oim* compared to control *oim* (15.1 ± 0.1 mm and 15.2 ± 0.1 mm respectively), with both being shorter than wild-type tibia (17.0 ± 0.1 mm, $P<0.001$) (Fig. 4A). The diameter of the tibia at the mid-diaphysis was also similar in transplanted and control *oim* (1.01 ± 0.01 mm and 1.05 mm respectively) but less than in wild-types (1.28 ± 0.02 mm, $P<0.001$) (Fig. 4B). The cortical bone thickness was decreased in *oim* compared to wild-type ($17.9\%\pm0.5\%$ and $20.4\%\pm0.3\%$, $P<0.001$ respectively), and was similar in untransplanted and transplanted *oim* mice ($17.9\%\pm0.5\%$ vs. $17.2\%\pm0.5\%$) (Fig. 4C).

Cortico-endosteal BFR was greater in wild-type mice compared with *oim* ($2.4\pm0.21\ \mu m^3/\mu m^2$/day SEM vs. $1.54\pm0.23\ \mu m^3/\mu m^2$/day SEM, $P<0.05$ respectively) (Fig. 4D). This difference resulted from an increased MAR at the cortico-endosteal interface ($2.6\pm0.3\ \mu m$/day vs. $1.7\pm0.3\ \mu m$/day, $P<0.05$ respectively) (Supplementary Fig. S2A) because there was no difference in MS ($92\%\pm2\%$ vs. $90\%\pm2\%$, respectively) (Supplementary Fig. S2B). The MAR and MS, however, did not differ between transplanted and nontransplanted *oim* mice (Fig. 4D and Supplementary Fig. S2A, B).

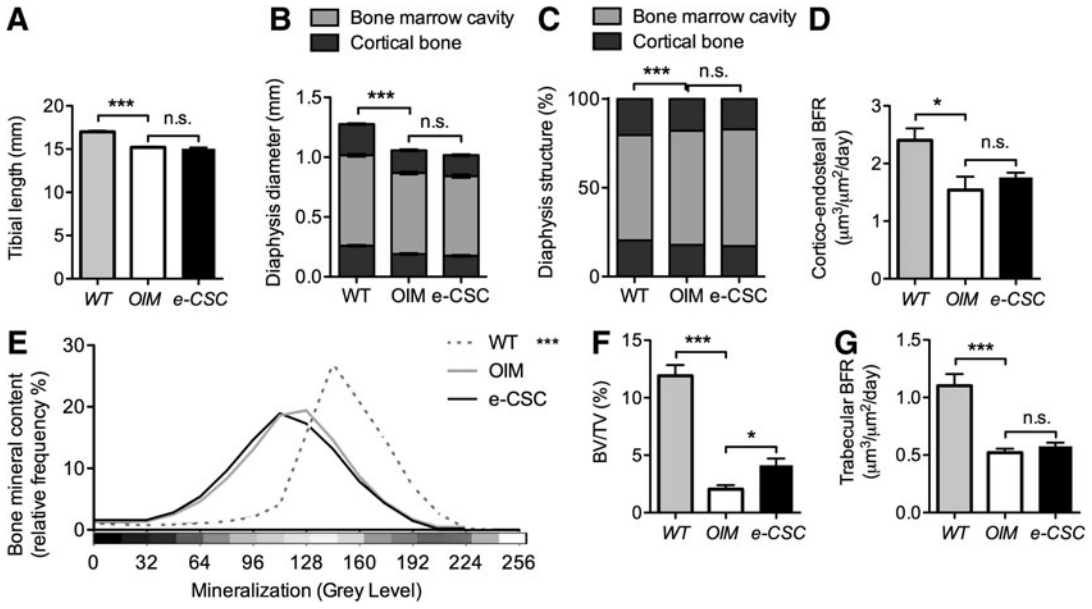

FIG. 4. Increased bone volume per total tissue volume (BV/TV) but not bone mineral content (BMC). **(A)** Tibial length (mm) for 8-week-old wild-type (WT; *gray*), nontransplanted *oim* (OIM; *white*) and e-CSC transplanted *oim* (e-CSC; *black*). **(B)** Tibial periosteal diameter (mm) at the mid shaft for each group showed medullary bone marrow cavity (*light gray*) and cortical bone (*dark gray*). **(C)** Relative thickness of tibial cortex compared to periosteal diameter. **(D)** Bone formation rate (BFR; $\mu m^3/\mu m^2$/day) for the endosteal cortex calculated from dual calcein labeling. **(E)** BMC shown as relative frequency (%) across 16 equal intervals of mineralization density [Displayed as a pseudocolor scheme where 0 gray level (*black*): low mineralization; 256 gray level (*white*): maximum mineralization]. **(F)** Percentage of trabecular bone volume in the tibial metaphysis per total tissue volume (BV/TV). **(G)** BFR ($\mu m^3/\mu m^2$/days) for trabecular bone calculated from dual calcein labeling. ns, not significant; $^*P<0.05$, $^{***}P<0.001$; Student's *t*-test or Kolmogorov–Smirnov test. Error bars are SEM.

Transplantation increases trabecular BV, but not BMC

The total BMC of combined trabecular and cortical bone compartments did not differ between transplanted and nontransplanted *oim* mice, both of which had markedly reduced BMC compared with wild-type ($P < 0.001$) (Fig. 4E and Supplementary Fig. S3). Trabecular BV/TV, however, was increased in transplanted compared with nontransplanted *oim* mice (4.1% ± 0.6% BV/TV vs. 2.0% ± 0.4% BV/TV respectively, $P < 0.05$), but remained lower than in wild-type mice (11.9% ± 0.9%) (Fig. 4F). Nevertheless, trabecular BFR did not differ between transplanted and nontransplanted *oim* mice ($0.58 \pm 0.03\,\mu m^3/\mu m^2/day$ vs. $0.52 \pm 0.03\,\mu m^3/\mu m^2/day$ respectively) and was reduced compared with wild-type ($1.10 \pm 0.1\,\mu m^3/\mu m^2/day$, $P < 0.001$) (Fig. 4G). Further, transplanted and nontransplanted *oim* had similar trabecular bone MAR ($0.86 \pm 0.04\,\mu m/day$ vs. $0.89 \pm 0.04\,\mu m/day$, $P < 0.05$ respectively) that was reduced compared with wild-type ($1.62 \pm 0.09\,\mu m/day$, $P < 0.001$) (Supplementary Fig. S4A). MS/BS did not differ between transplanted *oim*, nontransplanted *oim*, and wild-type mice (Supplementary Fig. S4B).

Transplantation reduces endogenous Smad3 expression and increases expression of genes activated during endochondral ossification

The mouse osteogenesis array (SABiosciences) was used to analyze changes in endogenous gene expression within the femoral epiphysis, and showed a global increase in expression of cartilage gene groups in e-CSC transplanted mice compared with nontransplanted *oim* controls (Fig. 5A). This included upregulation of genes involved in the early stages of endochondral ossification: 2.7-fold for *Sox9* ($P < 0.01$), 1.6-fold for *Twist1* ($P < 0.05$), 6.8-fold for *Col2α1* ($P < 0.01$), and 3.3-fold for *Col11α1* ($P < 0.05$). In addition, late hypertrophic chondrocyte differentiation genes were upregulated 4.4-fold for *Col10α1* ($P < 0.05$) and 2.6-fold for alkaline phosphatase ($P < 0.05$) [36], while chondrocyte assembly gene *Comp* was also upregulated 1.7-fold ($P < 0.05$) [37].

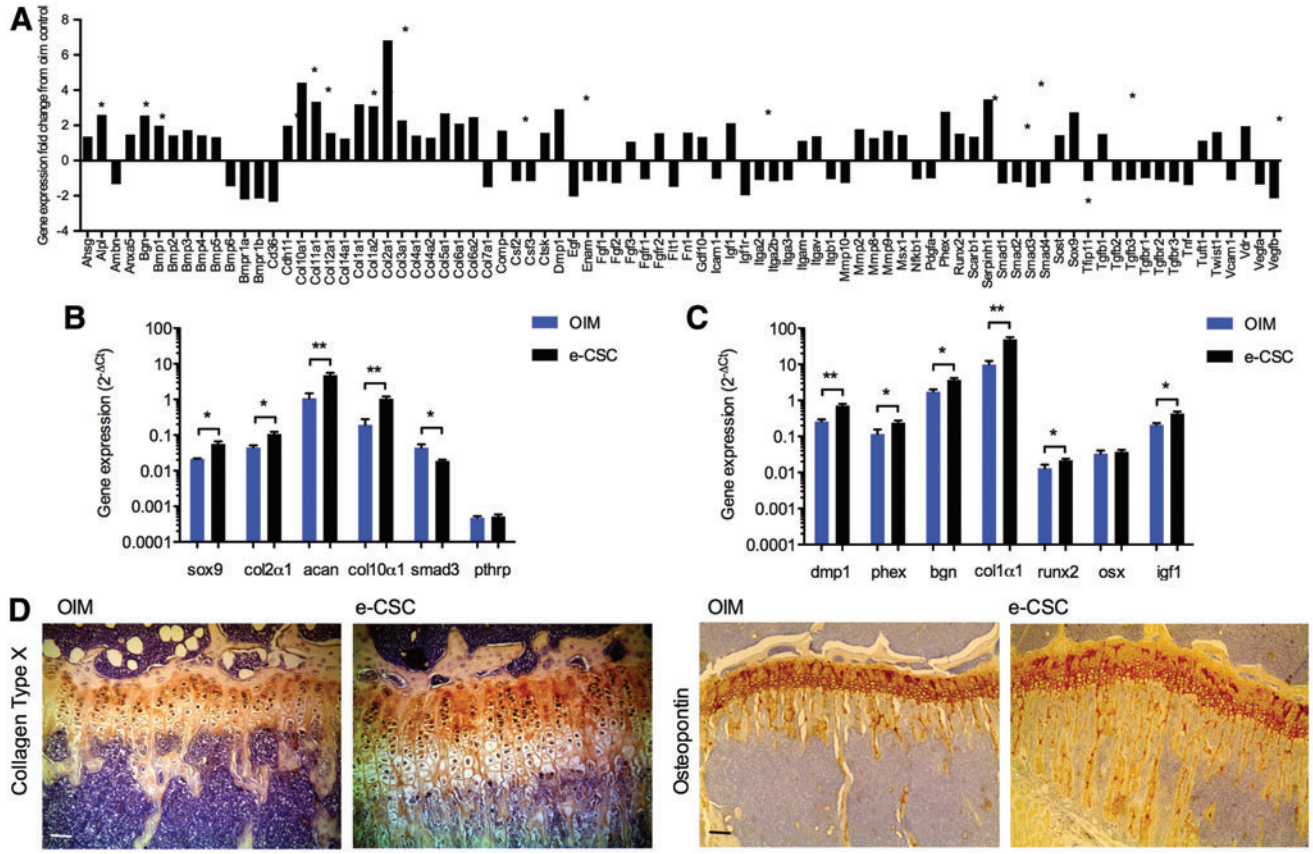

FIG. 5. Transplanted *oim* have increased expression of genes involved in endogenous osteogenesis and chondrogenesis. **(A)** Fold changes in gene expression in the femoral epiphysis of *oim* transplanted with e-CSC when compared to nontransplanted *oim* controls, generated from a mouse osteogenesis PCR array (SABiosciences). **(B)** Expression of genes involved in endochondral ossification; *Sox9*, *Col2α1*, *Aggrecan* (*Acan*), *Col10α1*, *Smad3*, and *Pthrp*. **(C)** Expression of genes involved in intramembranous ossification; *Dmp1*, *Phex*, *Biglycan* (*Bgn*), *Col1α1*, *Runx2*, *Osterix* (*Osx*), and *Igf1*. Results are given as $2^{-\Delta Ct}$ normalized to mouse *β-actin* and *hsp90ab1* for nontransplanted *oim* (*OIM*; *blue*) and *oim* transplanted with e-CSC (e-CSC; *black*). $^*P < 0.05$, $^{**}P < 0.01$; Student's *t*-test. Error bars are SEM. **(D)** Visualization of Collagen Type X with DAB staining (*brown*) in the tibial epiphysis of *oim* neonatally transplanted with e-CSC, compared to age-matched nontransplanted *oim* controls. Scale bar 100 μm. **(E)** Visualization of Osteopontin with DAB staining (*brown*) in the tibial epiphysis of *oim* neonatally transplanted with e-CSC, compared to age-matched nontransplanted *oim* controls. Scale bar 100 μm. Color images available online at www.liebertpub.com/scd

The array results were confirmed (Fig. 5B) by qRT-PCR for the key chondrogenesis transcription factor *Sox9* ($5.6\times10^{-2}\pm0.1\times10^{-2}\cdot2^{-\Delta Ct}$ in transplanted *oim* vs. $2.1\times10^{-2}\pm0.01\times10^{-2}\cdot2^{-\Delta Ct}$ in *oim* controls, $P<0.05$) [38]. Downstream upregulation of the *Sox9* transactivation target *Col2α1* [39,40] was also confirmed in transplanted *oim* compared to *oim* controls ($0.11\pm0.01\cdot2^{-\Delta Ct}$ vs. $0.04\pm0.01\cdot2^{-\Delta Ct}$ respectively, $P<0.05$) and of the key cartilage matrix component aggrecan [41,42] ($4.8\pm0.8\cdot2^{-\Delta Ct}$ vs. $1.1\pm0.4\cdot2^{-\Delta Ct}$ respectively, $P<0.01$), found in proliferating chondrocytes. However, expression of the *Sox9* target gene *Pthrp*, which inhibits chondrocyte maturation [43–45], was similar in transplanted and nontransplanted *oim* ($5.2\times10^{-4}\pm0.7\times10^{-4}\cdot2^{-\Delta Ct}$ vs. $4.8\times10^{-4}\pm0.5\times10^{-4}\cdot2^{-\Delta Ct}$). Importantly, *Smad3*, which inhibits maturation of chondrocytes by mediating TGF-β signaling [46], was downregulated in e-CSC transplanted mice compared with *oim* controls ($1.8\times10^{-2}\pm0.1\times10^{-2}\cdot2^{-\Delta Ct}$ vs. $4.4\times10^{-2}\pm1.1\times10^{-2}\cdot2^{-\Delta Ct}$ respectively, $P<0.05$). This correlated with increased expression of *Col10α1*, a marker of chondrocyte maturation [47], in transplanted mice compared to nontransplanted *oim*, ($1.0\pm0.2\cdot2^{-\Delta Ct}$ vs. $0.2\pm0.1\cdot2^{-\Delta Ct}$ respectively, $P<0.01$).

Upregulation of genes activated during intramembraneous ossification in transplanted mice is associated with increased endogenous expression of Runx2

The PCR array also identified genes involved in intramembraneous ossification that were upregulated in transplanted mice compared with *oim* controls. There was a 2.8-fold ($P<0.05$) increase in *Phex* and a 2.9-fold ($P<0.05$) increase in *Dmp1*, genes that are co-expressed by osteoblasts and osteocytes and regulate osteoblast maturation and bone mineralization via FGFR signaling pathways [48,49]. Also, upregulated in transplanted *oim* was *Bgn*, which has a role in osteoblast differentiation and matrix mineralization [50], and *Serpinh1*, which acts as a molecular chaperone in collagen biosynthesis [51] (2.6-fold, $P<0.05$, and 3.5-fold, $P<0.05$ respectively). These findings correlated with higher expression of extracellular matrix proteins in transplanted mice, including a 3.2-fold increase in *Col1α1* ($P<0.01$), involved in fibril formation of the abundant collagen type I [1,52] (Fig. 5A).

Array results were confirmed by qRT-PCR and showed *Runx2* expression, essential for osteoblast differentiation [53–55], was also increased in transplanted mice compared with nontransplanted *oim* ($2.1\times10^{-2}\pm0.2\times10^{-2}\cdot2^{-\Delta Ct}$ vs. $1.3\times10^{-2}\pm0.3\times10^{-2}\cdot2^{-\Delta Ct}$ respectively, $P<0.05$) (Fig. 5C). However, expression of the downstream transcription factor osterix, also required for osteoblast differentiation [56,57] was similar in both e-CSC transplanted *oim* and nontransplanted controls ($3.7\times10^{-2}\pm0.5\times10^{-2}\cdot2^{-\Delta Ct}$ vs. $3.3\times10^{-2}\pm0.7\times10^{-2}\cdot2^{-\Delta Ct}$ respectively). In contrast *Igf1*, which regulates both osteoblasts [58] and osteoclastogenesis via induction of RANK-L synthesis [59,60] and stimulates linear growth [61] was upregulated in transplanted mice ($0.43\pm0.05\cdot2^{-\Delta Ct}$ vs. $0.21\pm0.02\cdot2^{-\Delta Ct}$ for *oim* controls, $P<0.05$).

Expression of endogenous ossification genes correlated linearly with their co-activators and trans-activation targets as expected when mice were analyzed on an individual basis. For example, *Sox9* expression was positively correlated with expression of its transactivation target *Col2α1* ($R^2=0.84$) ($P<0.001$) (Supplementary Fig. S5A). Likewise, expression of the co-activators *Dmp1* and *Phex* were strongly correlated ($R^2=0.91$, $P<0.001$) (Supplementary Fig. S5B), as was expression of the ECM genes *Col1α1* and *Bgn* ($R^2=0.93$, $P<0.001$) (Supplementary Fig. S5C). Protein evaluation was performed in situ by immunohistochemistry, confirming increased expression of cartilage hypertrophic marker Collagen Type X and increased expression of the osteoblastic marker Osteopontin in mice treated with e-CSC compared to nontreated mice (Fig. 5D, E)

Growth plate height is increased in e-CSC transplanted oim

Analysis of growth plate height confirmed previous findings [15] that *oim* have larger growth plates than wild-type mice (153 ± 7 μm vs. 137 ± 9 μm respectively, $P<0.05$). Interestingly, e-CSC transplanted *oim* had a substantially wider growth plate (184 ± 6 μm) than *oim* controls ($P<0.05$), primarily the result of a larger hypertrophic zone (84 ± 4 μm for e-CSC transplanted *oim* vs. 60 ± 7 μm for *oim* controls, $P<0.01$) (Fig. 6A, B). When the relative proportions of the growth plate zones were calculated, the hypertrophic zone formed a larger proportion of the total growth plate in the transplanted mice than in nontransplanted *oim* mice ($46.4\%\pm1.1\%$ vs. $39.5\%\pm3.2\%$ respectively, $P<0.05$), in which the hypertrophic zone was similar to wild-type ($41.7\%\pm1.2\%$) (Fig. 6C). This finding was consistent with gene expression studies demonstrating that transplanted *oim* had a 10:1 ratio of expression of the late hypertrophic chondrocyte marker *Col10α1* in the epiphysis compared to expression of the proliferating chondrocyte marker *Col2α1*, whereas in nontransplanted *oim* the ratio was 4:1 ($P<0.05$).

There was a positive correlation ($R^2=0.75$, $y=20.13\times-0.84$, $P<0.01$) between endogenous *Col10α1* expression and the size of the hypertrophic zone of chondrocytes in the growth plate (Fig. 6D). *Runx2* expression was also correlated with the expression of *Col10α1* ($R^2=0.76$, $y=65.56\times-0.41$, $P<0.001$) (Fig. 6E) and may therefore be involved in mediating the larger hypertrophic zone in the growth plate. We also show a strong correlation between *Igf1* and *Bgn* expression ($R^2=0.89$, $y=8.64\times-0.15$, $P<0.001$), highlighting the importance of *Igf1* in regulating genes activated during intramembraneous ossification (Fig. 6F).

We next wanted to provide mechanistic clues as to how e-CSC transplantation induces upregulation of endogenous genes involved in skeletogenesis. We hypothesized that donor cells produce growth factors that stimulate maturation of endogenous chondrocyte progenitors. To test this hypothesis, we cultured e-CSC with the chondrogenic cell line ATDC5 to investigate whether e-CSC would produce factors that stimulate chondrogenic differentiation and maturation of ATDC5 cells. Although expression of the chondrogenic marker *Sox9* was higher in ATDC5 cells cultured in chondrogenic differentiated medium compared with levels found in noninduced cells, *Sox9* levels were not upregulated when ATDC5 cells were co-cultured without cell contact with e-CSC, indicating that e-CSC do not produce soluble factors that induce chondrocyte maturation in vitro (Fig. 6G). Interestingly, although ELISA analysis showed e-CSC did not produce bFGF, CTGF, and PDGF-BB when cultured in D10

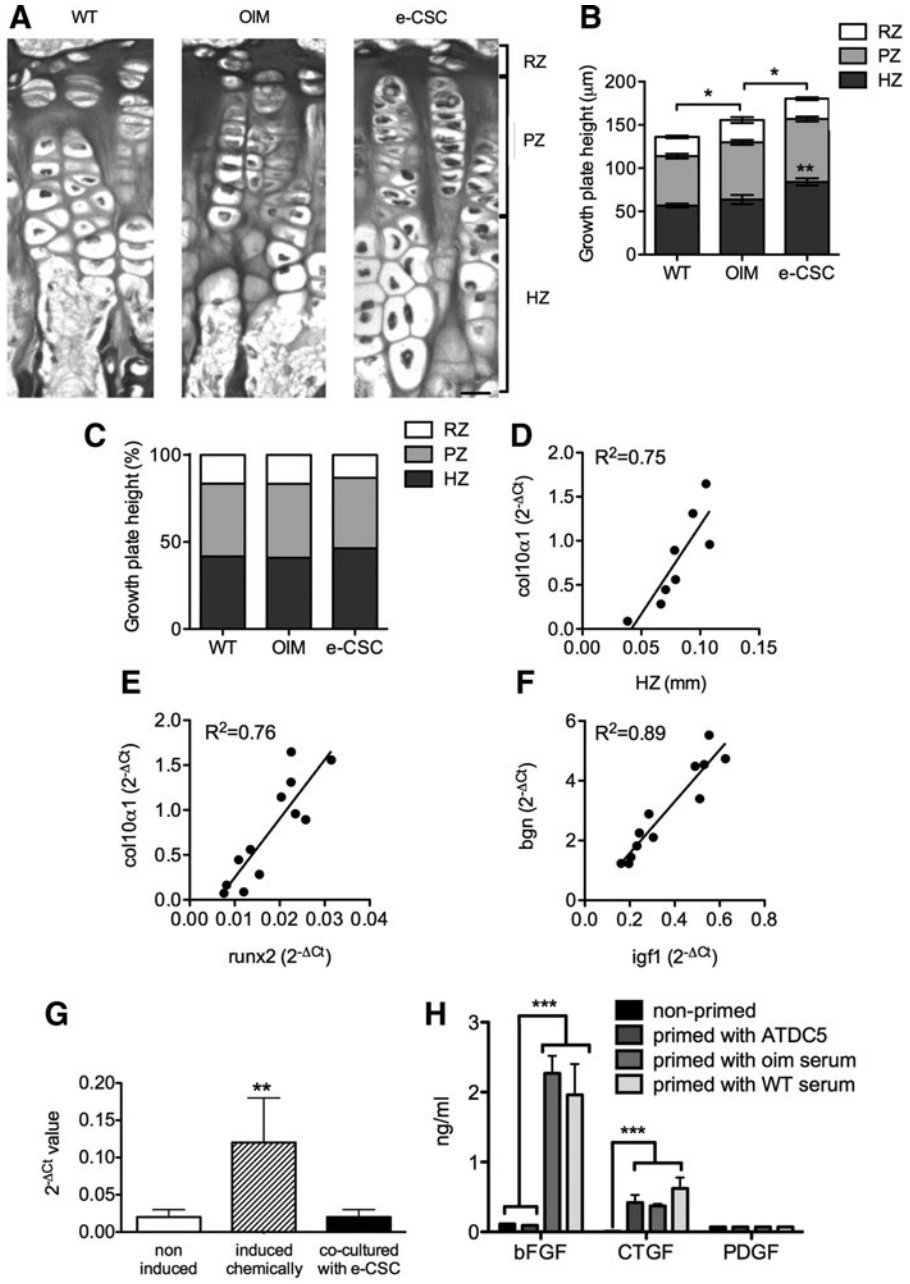

FIG. 6. Transplantation increases hypertrophic chondrocytes. **(A)** Tibial growth plate architecture of 8-week-old wild-type (WT), nontransplanted *oim* (OIM) and *oim* transplanted with e-CSC (e-CSC). Chondrocyte matrix is stained and contains a reserve zone (RZ) of cells undergoing clonal expansion, a proliferative zone (PZ) containing columns of proliferating chondrocytes, and a hypertrophic zone (HZ) of differentiated hypertrophic chondrocytes. Scale bar is 20 μm. **(B)** Mean widths of the tibial growth plate and growth plate zones (RZ, PZ, and HZ). Significance shown for total growth plate height. ns, not significant; $^{*}P < 0.05$, $^{**}P < 0.01$; Student's *t*-test. Error bars are SEM. **(C)** Ratio of zones (RZ, PZ, and HZ) within the growth plate. **(D)** Correlation between *Col10α1* gene expression (given as $2^{-\Delta Ct}$ normalized to mouse *β-actin* and *hsp90ab1*) and width of the hypertrophic zone (HZ) of the growth plate. **(E)** Correlation of *Runx2* and *Col10α1* gene expression. **(F)** Correlation of *Igf1* and *Bgn* gene expression. Linear line of best fit given. **(G)** Sox9 expression in ATDC5 cells was measured by quantitative real-time RT-PCR using the $2^{-\Delta Ct}$ method. ATDC5 cells were cultured in D10 medium alone (noninduced), induced to differentiate chemically, or co-cultured without cell contact with e-CSC for 7 days. Samples were tested in triplicates, and results are shown as mean ± SD. $^{**}P < 0.01$, when compared to noninduced ATDC5 cells; ANOVA variance analysis. **(H)** Measurement of basic fibroblast growth factor (bFGF), connective tissue growth factor (CTGF), and platelet-derived growth factor-BB (PDGF-BB) by e-CSC either cultured in D10 medium alone (nonprimed), in co-culture with ATDC5 cells without cell contact (primed with ATDC5), or the presence of blood serum from *oim* (primed with *oim* serum) or wild-type mice (primed with WT serum). Samples were tested in triplicates, and results are shown as mean ± SD. $^{***}P < 0.001$ when compared to nonprimed e-CSC; ANOVA variance analysis.

medium, they produced CTGF, but not bFGF or PDGF-BB, when co-cultured with ATDC5 (Fig. 6H). When primed with *oim* or wild-type seri, e-CSC produced both bFGF and CTGF, but not PDGF-BB, indicating the cells might respond to in vivo signals present in blood serum (Fig. 6H).

Discussion

This study demonstrates that fetal stem cells derived from human fetal early chorionic stem cells (e-CSC) have therapeutic benefits in the OI mouse model (*oim*) as evidenced by a two-third decrease in long bone fracture incidence and decreased bone brittleness compared with nontransplanted controls. These results are in line with our previous studies [15,16,62]. Fracture reduction in e-CSC transplanted mice was attributed to an increase in bone plasticity, as previously demonstrated [23], and greater bone ductility. Changes to the bone mechanical properties of transplanted *oim* were most likely mediated by the exogenous cells since higher engraftment levels in bones correlated with decreased bone stiffness. This is in agreement with recent work from our group showing that upregulation of CXCR4 in transplanted fetal blood MSC increased cell homing to sites of injury via the CXCR4-SDF1 pathway [62,63], which subsequently increased donor cell engraftment in addition to bone plasticity and bone quality [62]. Transplanted e-CSC homed to areas of bone growth and fracture repair and expressed osteoblast differentiation genes *Osteopontin* and *Osteocalcin* and the COL1A2 protein, indicating their differentiation to functional osteoblasts. These findings are in agreement with previous studies in the *oim* model that demonstrated the direct differentiation of transplanted cells to osteoblasts [13–16] and subsequent improvements in disease pathology. In addition, we used the detection of human factor IX as an immunoassay to detect the presence of mouse anti-human antibodies in the serum of mice transplanted with human cells and we were able to show the absence of immune reaction against allogeneic cells.

The trabecular BV/TV of *oim* is lower than wild-type mice due to the impaired osteoblast differentiation of *oim* [64,65], which results in a high numbers of preosteoblasts that support greater osteoclast bone resorption [64]. *Oim* mice transplanted with e-CSC had a higher BV/TV than nontransplanted *oim*, despite BFR remaining the same, which could be due to differentiation of exogenous cells to normal osteoblasts that better regulate bone remodeling. Increased BV/TV may also result from an indirect effect of the transplanted cells on osteoblast differentiation as demonstrated by the upregulated expression of endogenous genes in transplanted *oim* that were associated with osteoblast differentiation, including *Dmp1*, *Phex*, and *Bgn* [48–50]. Others have also shown an effect of transplantation on endogenous osteoblast activity, for example, transplantation of osteogenic differentiated MSC in SCID mice resulted in increased bone being produced by host cells [66], and endogenous osteoblast numbers were increased after transplantation of term placental stem cells in a SCID-rab mouse model of medullary myeloma-associated bone loss [67]. We also showed upregulation in transplanted *oim* of endogenous chondrogenesis genes including chondrogenesis regulator *Sox9* [38] and *Runx2*, implicated in chondrocyte maturation through *Col10α1* transactivation [68]. Expression of chondrocyte maturation inhibitor *Smad3* [46] was downregulated in transplanted mice. These changes were associated with a larger zone of hypertrophic chondrocytes within the growth plate, and indicate transplantation may have increased endogenous endochondral ossification.

The larger growth plate of e-CSC transplanted *oim* compared to *oim* controls is in contrast to previous data with human first trimester fetal blood MSC that instead showed normalization of growth plate height in prenatally transplanted *oim* compared to controls [15]. This may suggest different mechanisms of action between different transplanted cell sources. For example, recent work by Horwitz et al. in *oim* mice suggested different sources of cells contributed through different mechanisms when used in cell therapy, with nonadherent bone marrow cells differentiating to osteoblasts that produced normal collagen, while bone marrow MSC increased lumbar vertebrae length via paracrine mechanisms on chondrocyte proliferation at the growth plate, possibly through release of soluble growth factors [69].

BMC measured at the whole bone scale did not increase in *oim* after transplantation of e-CSC, despite changes in bone mechanical properties. Others have shown the importance of the collagen matrix organization on bone mechanical properties [70,71] and recently we have shown using nanoindentation that compared to wild-type mice, *oim* have greater mineralization of a poorly organized matrix [72]. Therefore, exogenous cells may have affected the bone mineralization or improved organization of bone matrix collagen fibers in the *oim* bones at the microscopic matrix scale, potentially in response to production of normal COL1A2.

To test the hypothesis that e-CSC produce growth factors that promote endogenous chondrocyte progenitor maturation and differentiation, we co-cultured e-CSC with ATDC5 in vitro. Interestingly, co-culture with ATDC5 cells induces e-CSC to produce CTGF, which is known to induce chondrocytic proliferation, maturation, and hypertrophy in vitro [73]. Interestingly, when primed with blood serum, e-CSC produced both CTGF and bFGF. CTGF is also known for stimulating proliferation and differentiation of cultured osteoblastic cells, and bFGF, which stimulates proliferation in the perichondrium [72]. Together, these results suggest e-CSC respond to in vivo signals to produce CTGF and bFGF, which may stimulate endogenous osteogenesis and chondrogenesis.

In summary, our study demonstrates that fetal stem cells derived from first trimester chorionic tissue have the potential to treat OI.

Acknowledgments

This research was funded by the Henry Smith Charity, Action Medical Research, and the Genesis Research Trust. G.N.J. was supported by the Medical Research Council. H.A. was supported by Action Medical Research. D.M. was supported by Newlife Foundation. N.M.F. acknowledges funding from the National Health and Medical Research Council (Australia). P.D.C. was supported by Great Ormond Street Hospital Children's Charity.

Author Disclosure Statement

The authors declare no competing financial interests exist.

References

1. Dalgleish R. (1997). The human type I collagen mutation database. Nucleic Acids Res 25:181–187.
2. Cohen-Solal L, L Zylberberg, A Sangalli, M Gomez Lira and M Mottes. (1994). Substitution of an aspartic acid for glycine 700 in the alpha 2(I) chain of type I collagen in a recurrent lethal type II osteogenesis imperfecta dramatically affects the mineralization of bone. J Biol Chem 269:14751–14758.
3. Stoss H and P Freisinger. (1993). Collagen fibrils of osteoid in osteogenesis imperfecta: morphometrical analysis of the fibril diameter. Am J Med Genet 45:257.
4. Van Dijk FS, G Pals, RR Van Rijn, PG Nikkels and JM Cobben. (2010). Classification of osteogenesis imperfecta revisited. Eur J Med Genet 53:1–5.
5. Letocha AD, HL Cintas, JF Troendle, JC Reynolds, CE Cann, et al. (2005). Controlled trial of pamidronate in children with types III and IV osteogenesis imperfecta confirms vertebral gains but not short-term functional improvement. J Bone Miner Res 20:977–986.
6. Ward LM, F Rauch, MP Whyte, J D'Astous, PE Gates, et al. (2011). Alendronate for the treatment of pediatric osteogenesis imperfecta: a randomized placebo-controlled study. J Clin Endocrinol Metab 96:355–364.
7. Rauch F and FH Glorieux. (2004). Osteogenesis imperfecta. Lancet 363:1377–1385.
8. Horwitz EM, DJ Prockop, PL Gordon, WW Koo, LA Fitzpatrick, et al. (2001). Clinical responses to bone marrow transplantation in children with severe osteogenesis imperfecta. Blood 97:1227–1231.
9. Horwitz EM, PL Gordon, WK Koo, JC Marx, MD Neel, et al. (2002). Isolated allogeneic bone marrow-derived mesenchymal cells engraft and stimulate growth in children with osteogenesis imperfecta: implications for cell therapy of bone. Proc Natl Acad Sci USA 99:8932–8937.
10. Le Blanc K, C Gotherstrom, O Ringden, M Hassan, R McMahon, et al. (2005). Fetal mesenchymal stem-cell engraftment in bone after in utero transplantation in a patient with severe osteogenesis imperfecta. Transplantation 79:1607–1614.
11. Pereira RF, MD O'Hara, AV Laptev, KW Halford, MD Pollard, et al. (1998). Marrow stromal cells as a source of progenitor cells for nonhematopoietic tissues in transgenic mice with a phenotype of osteogenesis imperfecta. Proc Natl Acad Sci USA 95:1142–1147.
12. Panaroni C, R Gioia, A Lupi, R Besio, SA Goldstein, et al. (2009). In utero transplantation of adult bone marrow decreases perinatal lethality and rescues the bone phenotype in the knockin murine model for classical, dominant osteogenesis imperfecta. Blood 114:459–468.
13. Wang X, F Li and C Niyibizi. (2006). Progenitors systemically transplanted into neonatal mice localize to areas of active bone formation in vivo: implications of cell therapy for skeletal diseases. Stem Cells 24:1869–1878.
14. Li F, X Wang and C Niyibizi. (2007). Distribution of single-cell expanded marrow derived progenitors in a developing mouse model of osteogenesis imperfecta following systemic transplantation. Stem Cells 25:3183–3193.
15. Guillot PV, O Abass, JH Bassett, SJ Shefelbine, G Bou-Gharios, et al. (2008). Intrauterine transplantation of human fetal mesenchymal stem cells from first-trimester blood repairs bone and reduces fractures in osteogenesis imperfecta mice. Blood 111:1717–1725.
16. Vanleene M, Z Saldanha, KL Cloyd, G Jell, G Bou-Gharios, et al. (2011). Transplantation of human fetal blood stem cells in the osteogenesis imperfecta mouse leads to improvement in multiscale tissue properties. Blood 117:1053–1060.
17. Portmann-Lanz CB, A Schoeberlein, A Huber, R Sager, A Malek, et al. (2006). Placental mesenchymal stem cells as potential autologous graft for pre- and perinatal neuroregeneration. Am J Obstet Gynecol 194:664–673.
18. Poloni A, V Rosini, E Mondini, G Maurizi, S Mancini, et al. (2008). Characterization and expansion of mesenchymal progenitor cells from first-trimester chorionic villi of human placenta. Cytotherapy 10:690–697.
19. Barlow S, G Brooke, K Chatterjee, G Price, R Pelekanos, et al. (2008). Comparison of human placenta- and bone marrow-derived multipotent mesenchymal stem cells. Stem Cells Dev 17:1095–1107.
20. Soncini M, E Vertua, L Gibelli, F Zorzi, M Denegri, et al. (2007). Isolation and characterization of mesenchymal cells from human fetal membranes. J Tissue Eng Regen Med 1:296–305.
21. Li CD, WY Zhang, HL Li, XX Jiang, Y Zhang, et al. (2005). Isolation and identification of a multilineage potential mesenchymal cell from human placenta. Placenta [Epub ahead of print]; DOI: 10.1016/j.placenta.2005.08.003.
22. Yen BL, HI Huang, CC Chien, HY Jui, BS Ko, et al. (2005). Isolation of multipotent cells from human term placenta. Stem Cells 23:3–9.
23. Jones GN, D Moschidou, TI Puga-Iglesias, K Kuleszewicz, M Vanleene, et al. (2012). Ontological differences in first compared to third trimester human fetal placental chorionic stem cells. PLoS One 7:e43395.
24. Guillot PV, C Gotherstrom, J Chan, H Kurata, NM Fisk. (2007). Human first-trimester fetal MSC express pluripotency markers and grow faster and have longer telomeres than adult MSC. Stem Cells 25:646–654.
25. Bassett JH, A Boyde, PG Howell, RH Bassett, TM Galliford, et al. (2010). Optimal bone strength and mineralization requires the type 2 iodothyronine deiodinase in osteoblasts. Proc Natl Acad Sci USA 107:7604–7609.
26. Chappard D, S Palle, C Alexandre, L Vico and G Riffat. (1987). Bone embedding in pure methyl methacrylate at low temperature preserves enzyme activities. Acta Histochem 81:183–190.
27. Yongchang Y and Y Wang. (2013). ATDC5: An excellent in vitro model cell line for skeletal development. J Cell Biochem 114:1223–1229.
28. Dominici M, K Le Blanc, I Mueller, I Slaper-Cortenbach, F Marini, et al. (2006). Minimal criteria for defining multipotent mesenchymal stromal cells. The International Society for Cellular Therapy position statement. Cytotherapy 8:315–317.
29. Adewumi O, B Aflatoonian, L Ahrlund-Richter, M Amit, PW Andrews, et al. (2007). Characterization of human embryonic stem cell lines by the International Stem Cell Initiative. Nat Biotechnol 25:803–816.
30. Skottman H, M Mikkola, K Lundin, C Olsson, AM Stromberg, et al. (2005). Gene expression signatures of seven individual human embryonic stem cell lines. Stem Cells 23:1343–1356.
31. Gotherstrom C, O Ringden, C Tammik, E Zetterberg, M Westgren, et al. (2004). Immunologic properties of human fetal mesenchymal stem cells. Am J Obstet Gynecol 190:239–245.
32. McKee MD and A Nanci. (1996). Osteopontin: an interfacial extracellular matrix protein in mineralized tissues. Connect Tissue Res 35:197–205.
33. Lian JB, GS Stein, C Stewart, E Puchacz, S Mackowiak, et al. (1989). Osteocalcin: characterization and regulated

expression of the rat gene. Connect Tissue Res 21:61–68; discussion 69.
34. Ryoo HM, HM Hoffmann, T Beumer, B Frenkel, DA Towler, et al. (1997). Stage-specific expression of Dlx-5 during osteoblast differentiation: involvement in regulation of osteocalcin gene expression. Mol Endocrinol 11:1681–1694.
35. Chipman SD, HO Sweet, DJ McBride, Jr., MT Davisson, SC Marks, Jr., et al. (1993). Defective pro alpha 2(I) collagen synthesis in a recessive mutation in mice: a model of human osteogenesis imperfecta. Proc Natl Acad Sci USA 90:1701–1705.
36. James CG, LA Stanton, H Agoston, V Ulici, TM Underhill, et al. (2010). Genome-wide analyses of gene expression during mouse endochondral ossification. PLoS One 5:e8693.
37. Haleem-Smith H, R Calderon, Y Song, RS Tuan and FH Chen. (2012). Cartilage oligomeric matrix protein enhances matrix assembly during chondrogenesis of human mesenchymal stem cells. J Cell Biochem 113:1245–1252.
38. Bi W, JM Deng, Z Zhang, RR Behringer and B de Crombrugghe. (1999). Sox9 is required for cartilage formation. Nat Genet 22:85–89.
39. Bell DM, KK Leung, SC Wheatley, LJ Ng, S Zhou, et al. (1997). SOX9 directly regulates the type-II collagen gene. Nat Genet 16:174–178.
40. Lefebvre V, W Huang, VR Harley, PN Goodfellow and B de Crombrugghe. (1997). SOX9 is a potent activator of the chondrocyte-specific enhancer of the pro alpha1(II) collagen gene. Mol Cell Biol 17:2336–2346.
41. Tsuji Y, Y Shimada, T Takeshita, N Kajimura, S Nomura, et al. (2000). Cryptic dimer interface and domain organization of the extracellular region of metabotropic glutamate receptor subtype 1. J Biol Chem 275:28144–28151.
42. Muir H. (1995). The chondrocyte, architect of cartilage. Biomechanics, structure, function and molecular biology of cartilage matrix macromolecules. Bioessays 17:1039–1048.
43. Amano K, K Hata, A Sugita, Y Takigawa, K Ono, et al. (2009). Sox9 family members negatively regulate maturation and calcification of chondrocytes through up-regulation of parathyroid hormone-related protein. Mol Biol Cell 20:4541–4551.
44. Huang W, UI Chung, HM Kronenberg and B de Crombrugghe. (2001). The chondrogenic transcription factor Sox9 is a target of signaling by the parathyroid hormone-related peptide in the growth plate of endochondral bones. Proc Natl Acad Sci USA 98:160–165.
45. Huang W, X Zhou, V Lefebvre and B de Crombrugghe. (2000). Phosphorylation of SOX9 by cyclic AMP-dependent protein kinase A enhances SOX9's ability to transactivate a Col2a1 chondrocyte-specific enhancer. Mol Cell Biol 20: 4149–4158.
46. Ferguson CM, EM Schwarz, PR Reynolds, JE Puzas, RN Rosier, et al. (2000). Smad2 and 3 mediate transforming growth factor-beta1-induced inhibition of chondrocyte maturation. Endocrinology 141:4728–4735.
47. Arias JL, O Nakamura, MS Fernandez, JJ Wu, P Knigge, et al. (1997). Role of type X collagen on experimental mineralization of eggshell membranes. Connect Tissue Res 36 :21–33.
48. Martin A, S Liu, V David, H Li, A Karydis, et al. (2011). Bone proteins PHEX and DMP1 regulate fibroblastic growth factor Fgf23 expression in osteocytes through a common pathway involving FGF receptor (FGFR) signaling. FASEB J 25:2551–2562.
49. Lorenz-Depiereux B, M Bastepe, A Benet-Pages, M Amyere, J Wagenstaller, et al. (2006). DMP1 mutations in autosomal recessive hypophosphatemia implicate a bone matrix protein in the regulation of phosphate homeostasis. Nat Genet 38:1248–1250.
50. Wang X, K Harimoto, S Xie, H Cheng, J Liu, et al. (2010). Matrix protein biglycan induces osteoblast differentiation through extracellular signal-regulated kinase and Smad pathways. Biol Pharm Bull 33:1891–1897.
51. Christiansen HE, U Schwarze, SM Pyott, A Al Swaid, M Al Balwi, et al. (2010). Homozygosity for a missense mutation in SERPINH1, which encodes the collagen chaperone protein HSP47, results in severe recessive osteogenesis imperfecta. Am J Hum Genet 86:389–398.
52. Stacey A, J Bateman, T Choi, T Mascara, W Cole, et al. (1988). Perinatal lethal osteogenesis imperfecta in transgenic mice bearing an engineered mutant pro-alpha 1(I) collagen gene. Nature 332:131–136.
53. Ducy P, R Zhang, V Geoffroy, AL Ridall and G Karsenty. (1997). Osf2/Cbfa1: a transcriptional activator of osteoblast differentiation. Cell 89:747–754.
54. Komori T, H Yagi, S Nomura, A Yamaguchi, K Sasaki, et al. (1997). Targeted disruption of Cbfa1 results in a complete lack of bone formation owing to maturational arrest of osteoblasts. Cell 89:755–764.
55. Otto F, AP Thornell, T Crompton, A Denzel, KC Gilmour, et al. (1997). Cbfa1, a candidate gene for cleidocranial dysplasia syndrome, is essential for osteoblast differentiation and bone development. Cell 89:765–771.
56. Karsenty G and EF Wagner. (2002). Reaching a genetic and molecular understanding of skeletal development. Dev Cell 2:389–406.
57. Kurata H, PV Guillot, J Chan and NM Fisk. (2007). Osterix induces osteogenic gene expression but not differentiation in primary human fetal mesenchymal stem cells. Tissue Eng 13:1513–1523.
58. Giustina A, G Mazziotti and E Canalis. (2008). Growth hormone, insulin-like growth factors, and the skeleton. Endocr Rev 29:535–559.
59. Mochizuki H, Y Hakeda, N Wakatsuki, N Usui, S Akashi, et al. (1992). Insulin-like growth factor-I supports formation and activation of osteoclasts. Endocrinology 131:1075–1080.
60. Niu T and CJ Rosen. (2005). The insulin-like growth factor-I gene and osteoporosis: a critical appraisal. Gene 361:38–56.
61. Yakar S, CJ Rosen, WG Beamer, CL Ackert-Bicknell, Y Wu, et al. (2002). Circulating levels of IGF-1 directly regulate bone growth and density. J Clin Invest 110:771–781.
62. Jones GN, D Moschidou, K Lay, H Abdulrazzak, M Vanleene, et al. (2012). Upregulating CXCR4 in human fetal mesenchymal stem cells enhances engraftment and bone mechanics in a mouse model of osteogenesis imperfecta. Stem Cells Transl Med 1:70–78.
63. Granero-Molto F, JA Weis, MI Miga, B Landis, TJ Myers, et al. (2009). Regenerative effects of transplanted mesenchymal stem cells in fracture healing. Stem Cells 27:1887–1898.
64. Li H, X Jiang, J Delaney, T Franceschetti, I Bilic-Curcic, et al. (2010). Immature osteoblast lineage cells increase osteoclastogenesis in osteogenesis imperfecta murine. Am J Pathol 176:2405–2413.
65. Kalajzic I, J Terzic, Z Rumboldt, K Mack, A Naprta, et al. (2002). Osteoblastic response to the defective matrix in the osteogenesis imperfecta murine (oim) mouse. Endocrinology 143:1594–1601.

66. Zhou Y, W Fan, I Prasadam, R Crawford and Y Xiao. (2012). Implantation of osteogenic differentiated donor mesenchymal stem cells causes recruitment of host cells. J Tissue Eng Regen Med.
67. Li X, W Ling, A Pennisi, Y Wang, S Khan, et al. (2011). Human placenta-derived adherent cells prevent bone loss, stimulate bone formation, and suppress growth of multiple myeloma in bone. Stem Cells 29:263–273.
68. Zheng Q, G Zhou, R Morello, Y Chen, X Garcia-Rojas, et al. (2003). Type X collagen gene regulation by Runx2 contributes directly to its hypertrophic chondrocyte-specific expression in vivo. J Cell Biol 162:833–842.
69. Otsuru S, PL Gordon, K Shimono, R Jethva, R Marino, et al. (2012). Transplanted bone marrow mononuclear cells and MSCs impart clinical benefit to children with osteogenesis imperfecta through different mechanisms. Blood 120:1933–1941.
70. Zebaze RM, AC Jones, MG Pandy, MA Knackstedt and E Seeman. (2011). Differences in the degree of bone tissue mineralization account for little of the differences in tissue elastic properties. Bone 48:1246–1251.
71. Gupta HS, S Schratter, W Tesch, P Roschger, A Berzlanovich, et al. (2005). Two different correlations between nanoindentation modulus and mineral content in the bone-cartilage interface. J Struct Biol 149:138–148.
72. Vanleene M, A Porter, PV Guillot, A Boyde, M Oyen, et al. (2012). Ultra-structural defects cause low bone matrix stiffness despite high mineralization in osteogenesis imperfecta mice. Bone 50:1317–1323.
73. Frayssinet P, JL Jouve and E Viehweger. (2004). Cartilage cells. In: *Biomechanics and Biomaterials in Orthopaedics*. Thorngren KG, DG Poitout, R Kotz, eds. Springer, London, pp 219.

Address correspondence to:
Dr. Pascale V. Guillot
Institute of Reproductive and Developmental Biology
Imperial College London
Du Cane Road
London W12 0NN
United Kingdom

E-mail: pascale.guillot@imperial.ac.uk

Received for publication March 11, 2013
Accepted after revision September 12, 2013
Prepublished on Liebert Instant Online September 12, 2013